International Journal of
Translational Medicine

MDPI

Review

Geometric Misalignment in Corneal and Corneoscleral Imaging: From Acquisition Artefacts to Artificial Intelligence Validation

Rami Alanazi [1], Joseph Towler [2], Jay Davies [1], Akram Joda [3,*] and Ahmed Abass [1]

[1] Department of Materials, Design and Manufacturing Engineering, School of Engineering, University of Liverpool, Liverpool L69 3GH, UK; r.alanazi@liverpool.ac.uk (R.A.); hljdavi9@liverpool.ac.uk (J.D.); a.abass@liverpool.ac.uk (A.A.)
[2] Translational Clinical Eye Research Centre, Alder Hey Children's Hospital, Liverpool L14 5AB, UK; joseph.towler@alderhey.nhs.uk
[3] Faculty of Engineering, Higher Colleges of Technology, Dubai P.O. Box 15825, United Arab Emirates
* Correspondence: ajoda@hct.ac.ae

Abstract

Background: Corneal and corneoscleral maps are sensitive not only to acquisition pose but also to the coordinate frames, reference surfaces and transformations used in reconstruction and comparison. This narrative review examines geometric uncertainty as a connected measurement chain extending from imaging to clinical and artificial intelligence (AI) inference. Methods: A structured PubMed/MEDLINE search was supplemented by IEEE Xplore searching, citation tracking and cross-checking against publicly accessible Scopus- and Web of Science-indexed records. The literature cut-off was 15 September 2026. Evidence was appraised qualitatively as direct, near-direct or contextual rather than pooled across heterogeneous measurement methods. Results: Fixation error and ocular rotation can produce clinically misleading asymmetry; axis and reference-surface definitions change derived measurements, while registration reduces only the component of between-scan difference attributable to the fitted transform. Quantified effects are device-, surface- and task-dependent. AI studies report strong diagnostic discrimination in selected datasets, but validation of physical misalignment tolerance and clinical impact is substantially less developed. Conclusions: Geometric quality control must encompass acquisition, reference-frame definition, repeatability and downstream analysis. Patient-level evaluation, explicit laterality handling and deliberate geometric stress testing are necessary to assess AI robustness. Available evidence does not justify a universal tolerance for translation, rotation or tilt.

Keywords: corneal topography; corneal tomography; corneoscleral topography; misalignment; eye tilt; map registration; artificial intelligence; machine learning

Check for updates

Academic Editor: Pier Claudio

Received: 23 September 2026
Revised: 8 November 2026
Accepted: 17 November 2026
Published: 24 November 2026

Copyright: © 2026 by the authors. Licensee MDPI, Basel, Switzerland. This article is an open access article distributed under the terms and conditions of the Creative Commons Attribution (CC BY) license.

1. Introduction

Placido-disc systems infer anterior corneal curvature from reflected ring geometry, whereas slit-scanning, rotating Scheimpflug, and anterior-segment optical coherence tomography (OCT) systems reconstruct section-based or volumetric information that may include posterior elevation and pachymetry [1–3]. Wide-field profilers extend measurement beyond the central cornea and reconstruct the limbus and visible sclera from projected patterns [4–6]. Multi-gaze approaches enlarge coverage by combining measurements from different viewing positions [7]. Platform dependence reflects both the optical

signal and the sampled region [1–3]. It also reflects the chosen reference surface and reconstruction algorithm [8].

In this review, geometric misalignment means an incorrect or inconsistent relationship between the ocular surface, acquisition axis and coordinate system used for reconstruction or comparison [9–11]. It includes eccentric fixation and surface tilt [9,12,13], ocular or head rotation and normal micro-movements [9,14], and residual rigid-body mismatch between repeated maps [15]. Tear-film break-up and blink timing can also change a map [16,17], as can accommodation or a recent contact procedure [18,19]. These effects are potential confounders rather than registration errors and are considered separately.

Acquisition error and between-scan registration error should be distinguished [9,15,20]. Off-axis capture can distort a single map at the time of measurement [9,12]. Two otherwise valid maps may appear different when their coordinate systems are not aligned before subtraction [15,20]. The first problem can affect diagnosis from one examination [12]; the second can affect claims of progression or treatment response [21–23].

Early clinical studies showed that fixation errors could produce inferior–superior asymmetry and pseudokeratoconus-like patterns [12]. Later experiments examined surface tilt and rotation [9,13], line-of-sight mismatch [10], and normal ocular micro-movements [14]. More recent work has used the limbus as a three-dimensional landmark and levelled wide-field data to a limbal plane [5,6], quantified the effect of tilt on fitted asphericity and densitometry [24,25], and compared stitched multi-gaze maps with single-shot profilometry [7].

The distinction matters in ectasia screening because geometric artefact can resemble pathological asymmetry [9,12]. It also matters when serial maps are used to judge postoperative or disease-related change [21–23] and when corneoscleral maps are re-centred for contact-lens assessment [26]. A method that reduces a numerical surface difference is not necessarily clinically beneficial if it also suppresses focal disease or preserves an acquisition artefact. Translation into practice therefore requires evidence that a correction improves the intended decision, not only a map's appearance or repeatability.

Scope and Contribution

Broad reviews have described imaging platforms and their clinical applications [1–3]. Work on acquisition geometry and platform dependence has developed in a more specialised literature [6,8], while between-scan registration has largely been treated as a separate methodological problem [15,20]. This review's novelty is to connect these problems as one measurement chain from acquisition to clinical decision, as shown in Figure 1. The framework separates acquisition error, coordinate correction and biological change; grades evidence by causal proximity; and asks whether artificial intelligence resolves, inherits, or obscures geometric uncertainty. It also converts the synthesis into minimum reporting information for longitudinal assessment, ectasia and refractive services, and wide-field contact-lens practice.

Viewed chronologically, the evidence developed along three partly overlapping lines: optical reconstruction and controlled fixation or rotation experiments in 1991–2007 [9–14]; registration, geometric fitting and landmark-based levelling in 2014–2021 [5,6,15,20,27,28]; and contemporary work on multi-gaze imaging, device-specific precision and AI-based interpretation in 2024–2026 [7,29–37]. These lines of evidence address different questions—how geometric pose changes a measurement, how coordinate operations influence agreement, and whether a derived measurement supports clinical decisions—and should not be treated as interchangeable forms of validation.

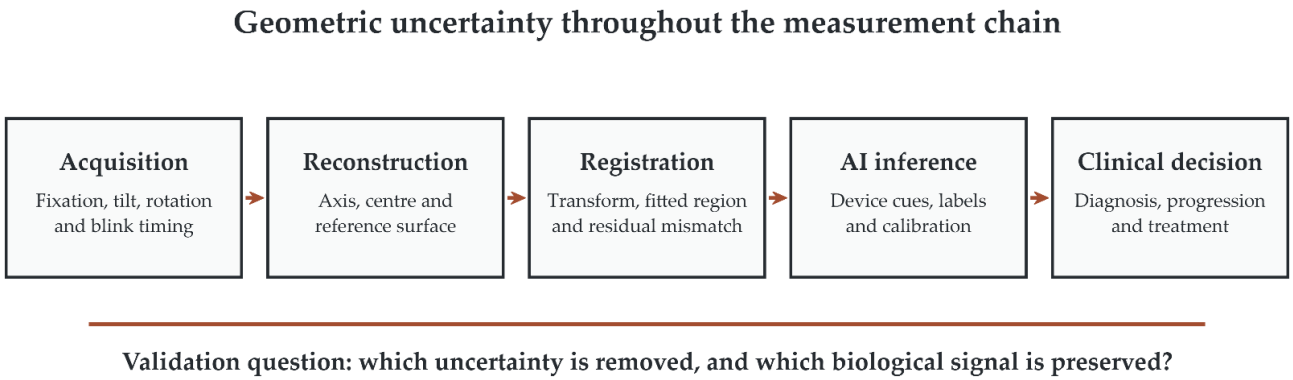


Figure 1. Proposed measurement-chain framework. Geometric uncertainty can enter during acquisition, be transformed during reconstruction and registration, and be inherited or amplified by artificial intelligence before reaching a clinical decision. Each correction should therefore be judged by the uncertainty it removes and the biological signal it preserves. The figure was created using MATLAB R2025b (MathWorks, Natick, MA, USA).

2. Review Approach

This narrative review used structured literature searches to support a critical qualitative synthesis, with an overall literature cut-off of 15 September 2026. PubMed/MEDLINE was the principal biomedical source, supplemented by IEEE Xplore searching, backward and forward citation tracking, and bibliographic cross-checking of publications indexed in Scopus and Web of Science through accessible publisher and index records. The included articles were published between 1991 and 2026.

The two title/abstract PubMed/MEDLINE search expressions were recorded and reproduced verbatim in Supplementary Table S1. The first combined corneal or corneoscleral topography and tomography terms with misalignment, fixation, decentration, tilt, rotation, translation, visual or geometric axes, limbal landmarks, levelling, registration, stitching, repeatability and agreement. The second combined keratoconus or corneal ectasia with artificial intelligence or machine learning and corneal imaging terms. Additional engineering and AI studies were considered through the supplementary sources described in Table S1.

Supplementary engineering searches used related concepts adapted to the source. Boolean NOT operators were not used; instead, records were assessed against the eligibility criteria during title/abstract screening and, where relevant, full-text review. This preserved studies addressing ocular geometry alongside broader imaging or computational topics. Table S1 provides the original PubMed queries, the roles of the supplementary sources, and the study-selection approach. Scopus and Web of Science were used for bibliographic cross-checking rather than claimed as separate systematic database screens.

Eligibility was assessed first from titles and abstracts and then, where indicated, from full texts. Peer-reviewed journal articles were included when they imposed, simulated, measured or estimated geometric error, or examined the influence of reference axes, levelling or between-map registration on ocular-surface measurements. AI studies were eligible when corneal topography, tomography or anterior-segment OCT formed a substantive input. Device-comparison, progression and confounder studies were included as contextual evidence. Conference abstracts, book chapters, manufacturer material and non-journal web sources were excluded. The qualitative synthesis included 59 journal articles; three additional reporting-guideline references informed the proposed checklist. Evidence was classified by its proximity to a geometric mechanism. Direct studies experimentally imposed a transformation or estimated an acquisition or between-scan misalignment and measured its effect. Near-direct studies isolated a geometric modelling choice, such as a coordinate

axis, limbal landmark, fitted reference surface or registration transform. Contextual studies addressed repeatability, inter-device agreement, confounding, disease progression or AI discrimination without isolating misalignment as the causal variable. Because transformation variables, devices, surfaces, fitted regions and clinical endpoints differed substantially, a quantitative meta-analysis would combine non-equivalent outcomes; evidence was therefore synthesised narratively, with comparable magnitudes retained in Table 1. Neither a PRISMA flow diagram nor a formal risk-of-bias instrument was used, and the conclusions should not be interpreted as those of a systematic review.

Table 1. Direct and near-direct evidence on geometric misalignment.

Study and Platform	Perturbation or Estimated Pose	Design	Quantified Measurement Effect	Interpretation
Hubbe and Foulks; EyeSys [12]	Fixation at 0°, 2.5°, 5° and 10° below axis	Five eyes and three aspheric surfaces	I–S asymmetry increased; significant at 5° ($p < 0.05$); keratoconus-like patterns below 5° in some eyes	Controlled acquisition error can imitate pathology
Douthwaite and Pardhan; EyeSys [13]	10° eccentric fixation; central-fixation tilt estimated at ≈3.2–3.3°	Two experiments with 24 participants each	Tilt explained a substantial share of nasal–temporal asymmetry; no comparable universal curvature change reported	Apparent asymmetry depends on ocular orientation
Salmon and Thibos; VK + aberrometry [10]	Instrument axis versus line of sight; displacement not tabulated here	Corneal/whole-eye optical analysis	Corneal and inferred internal aberration estimates changed; a uniform numeric effect is not available	Requires a common measurement axis
Buehren et al.; videokeratoscopy [14]	Estimated tilt, displacement and cyclotorsion; per-component magnitude not extracted	20 maps from each of 10 participants	Mean RMS map error reduced by 24.6% after repositioning	Residual natural pose variability is measurable
Hick et al.; Orbscan II [9]	Vertical and horizontal induced rotation/translation; numeric angles not available in abstract	29 healthy subjects and optical modelling	Rotation significantly changed asymmetry indices and several fit parameters; translation had smaller effects	Effect magnitude cannot be extrapolated to other systems
Bao et al.; Pentacam [15]	Estimated between-map pose: SD x/y ≈ 49/54 µm; angular SD ≈ 0.41°/0.37°/2.35°	Paired maps from 124 healthy eyes; six-DOF ICP	Combined RMS 8.46 ± 2.75 → 7.28 ± 2.58 µm; anterior 4.58 ± 1.84 → 2.97 ± 1.29 µm	Correction reduces, but does not abolish, map discrepancy
Schröder et al.; tomography comparison [8]	Platform-specific alignment component; no single imposed magnitude	Cross-platform repeated-map comparison	Correction effect differed with measurement principle; no common effect size	Platform-specific inference is required

Note: Values are transcribed from the cited studies where available; 'not extracted' or 'not available' does not denote a measured zero. Different outcomes and instruments preclude direct pooling. I–S, inferior–superior; VK, videokeratoscopy; RMS, root mean square; ICP, iterative closest point; DOF, degrees of freedom.

3. Geometric Framework

Three coordinate frames must be distinguished: an instrument frame I fixed to the acquisition system, an ocular frame O defined by explicit anatomical or optical landmarks, and an analysis frame A in which derived measurements or between-visit comparisons are expressed [10,11,27]. A sampled surface point is not defined by its coordinates alone; its location depends on the origin, axis directions, handedness and units of the adopted frame. If the relative pose is treated as rigid, a point measured in I can be represented in A by the rotation R and translation t specified below. Physical ocular pose during capture, the reconstruction convention used by a device and a computational between-map transform are distinct operations and should be reported separately [9,11,15,27].

When p_A represents the three-dimensional coordinates of a measured point on the corneal surface, where pI is the same physical point expressed in the instrument coordinate frame, then:

$$p_A = R_z(\gamma)\, R_y(\beta)\, R_x(\alpha)\, p_I + t \quad (1)$$

$$\text{where, } t = \left(t_x,\ t_y,\ t_z\right) \quad (2)$$

In Equations (1) and (2), $R_x(\alpha)$, $R_y(\beta)$ and $R_z(\gamma)$ denote right-handed active rotations about the stated x, y and z axes, applied in x–y–z order to column vectors; t is expressed in the destination frame. Under the illustrated convention, α describes pitch about x, β describes yaw about y and γ describes torsion about z, provided that the local axes are defined accordingly. Euler-angle names and signs depend on the adopted convention and should not be compared across studies without conversion. A fitted registration may estimate all six rigid-body components, whereas an off-axis scan can also introduce projection or reconstruction bias that no subsequent rigid transform can necessarily undo [9,11,15].

Geometrical and visual axes are not coincident in the normal eye [10,38]. Abass et al. mapped the relative positions of ocular geometrical and visual axes in Brazilian, Chinese and Italian populations. They described locating the visual centre with reference to the geometric axis [38]. Their findings reinforce that the term centre must be defined when decentration or alignment is reported [10,38].

Axis mismatch is particularly important when combining measurements from different instruments [10]. Salmon and Thibos showed that mismatch between the videokeratoscope axis and the line of sight altered estimates of corneal aberration, internal aberration and their relationship [10]. A corneal wavefront should therefore not be subtracted from a whole-eye wavefront unless the measurements use compatible reference axes or have been transformed into a common coordinate system [10].

Photokeratoscopic modelling showed that reconstruction accuracy is sensitive to astigmatism and misalignment [11]. Fitting studies using Scheimpflug elevation data also showed that allowing translation and rotation changes the fitted surface and derived topographic quantities [27]. These studies treat coordinate transformation as part of the measurement model rather than a neutral display option [11,27]. A null-screen study further showed that tilt and decentration can be estimated and corrected within a defined optical configuration, although the reported accuracy is specific to that system [39].

Reference-surface selection is a further geometric step, rather than a neutral display setting. An elevation map represents the residual between the reconstructed corneal surface and a chosen fitted reference, such as a best-fit sphere or another parametric surface. Altering the reference family, fitting-zone diameter, excluded regions, centre or alignment can change the elevation pattern without a corresponding change in tissue shape [8,27,40]. The fitting parameters and analysis zone must therefore be specified before maps or AI inputs derived from different systems are compared. The Belin/Ambrósio Enhanced Ectasia Display (BAD-D) should be distinguished from the reference surface itself: it is a composite ectasia

index incorporating elevation- and pachymetry-related information, including enhanced-reference-surface concepts, rather than a single fitted sphere [23,32,41].

Figure 2 distinguishes rigid coordinate transformation from the reference-surface choice used to calculate elevation residuals, whereas Figure 3 illustrates six acquisition and pose-mismatch modes. These steps must be kept conceptually separate: a lower fitted residual does not establish correction of the original acquisition artefact, and a different best-fit surface changes displayed elevation even when the registered point cloud is unchanged.

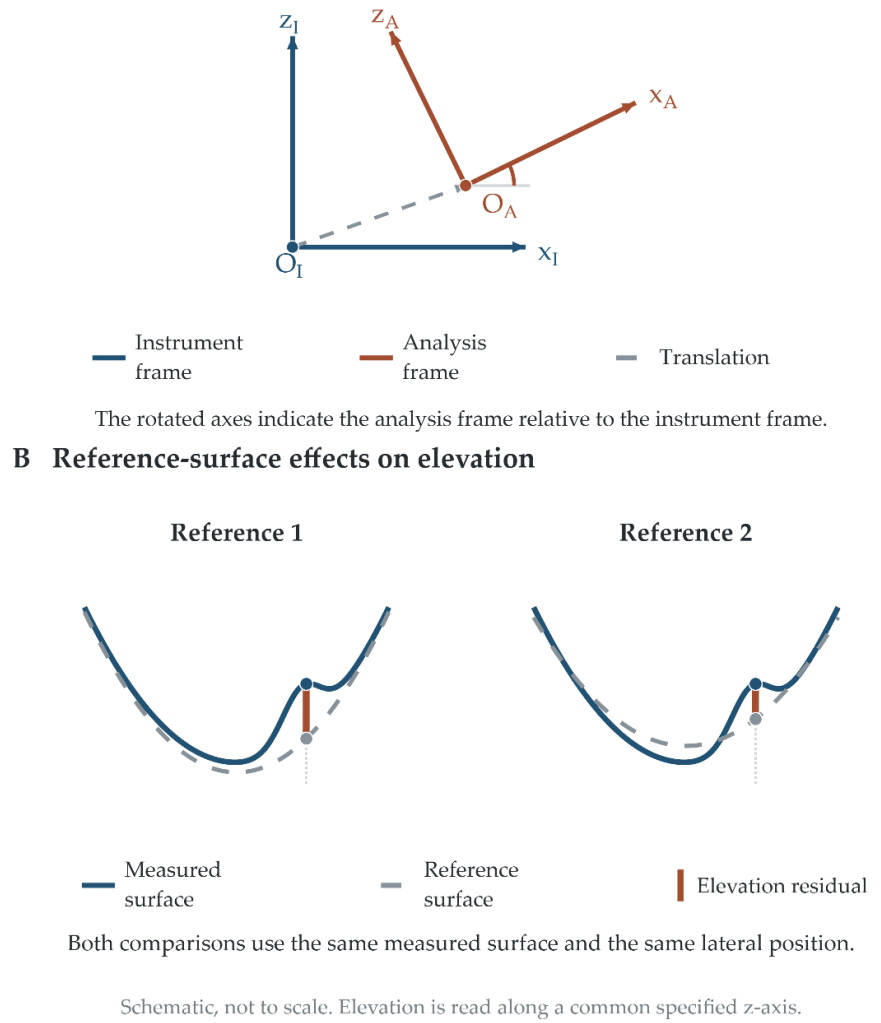


Figure 2. Geometric operations at distinct stages of the measurement chain. (**A**) Two-dimensional schematic of the instrument (I) and analysis (**A**) coordinate frames, showing their relative translation and rotation. (**B**) The same reconstructed ocular profile is compared with two illustrative reference surfaces at an identical lateral position. The vertical segments indicate the different elevation residuals obtained without changing the measured profile. The illustration is schematic, not to scale, and does not establish clinical misalignment limits. The figure was created using MATLAB R2025b (MathWorks, Natick, MA, USA).

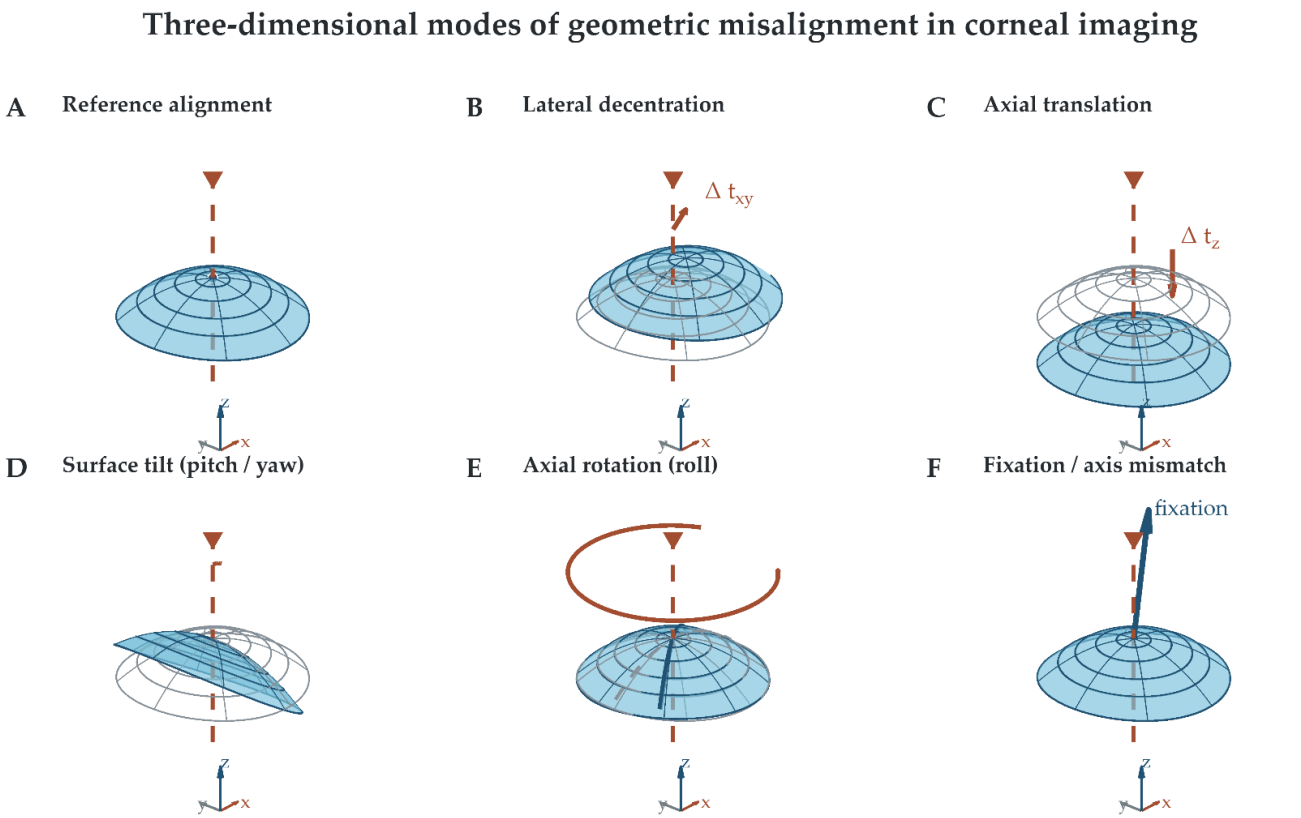


Figure 3. Three-dimensional schematic of major geometric misalignment modes in corneal and corneoscleral imaging. (**A**) Reference alignment; (**B**) lateral translation (decentration); (**C**) axial translation; (**D**) surface tilt about a transverse axis (pitch or yaw, depending on coordinate convention); (**E**) rotation about the instrument axis (roll); and (**F**) mismatch between the fixation direction and the instrument axis. The pale-blue surface represents the measured corneal pose, while the grey wireframe, where present, indicates the reference surface. The dashed orange line shows the instrument axis; arrows indicate the illustrated displacement, rotation or fixation direction. A small x–y–z coordinate triad is shown in each panel. The modes are schematic and may coexist. The figure was created using MATLAB R2025b (MathWorks, Natick, MA, USA).

4. Eccentric Fixation, Tilt and Rotation

Hubbe and Foulks measured five human corneas and three aspheric test surfaces with the visual axis displaced 0°, 2.5°, 5° and 10° below the videokeratoscope axis [12]. Inferior–superior curvature asymmetry increased with eccentric fixation, and keratoconus-like patterns were evident at deviations below 5° in some eyes; the increase in the asymmetry index was statistically significant at 5° [12]. These findings establish a direct acquisition mechanism for a false disease-like pattern, without defining a transferable tolerance for other instruments or surfaces.

Douthwaite and Pardhan compared central fixation with fixation 10° off-centre using the EyeSys videokeratoscope [13]. Estimated corneal tilt at central fixation was approximately 3.2–3.3° across their two experiments, supporting the interpretation that a substantial component of apparent nasal–temporal asymmetry could reflect surface orientation rather than anatomy [13]. Because the reported angle describes estimated tilt in that configuration, it should not be treated as a universal geometric-error threshold.

Hick et al. induced rotational and translational misalignment in healthy eyes measured with Orbscan II and supported the clinical experiment with mathematical modelling [9]. Rotation changed simulated keratometry and direction-specific asymmetry measures more consistently than the technician-induced translation used in that protocol [9]. Downward and horizontal rotations generated asymmetric curvature or elevation patterns that could resemble keratoconus [9]. The magnitude of these effects should not be transferred to other instruments as a universal tolerance [8,9].

Normal ocular micro-movements further affect repeated capture [14]. In 20 videokeratographs per participant for 10 participants, Buehren et al. estimated displacement, tilt and cyclotorsion and reported a 24.6% mean reduction in root mean square (RMS) map discrepancy after repositioning [14]. Individual pose-component magnitudes are not quoted here because they were not extractable from the accessible summary. Table 1 distinguishes imposed or estimated misalignment magnitude from the resulting measurement change wherever the source permits.

5. Landmark-Based Levelling and Wide-Field Eye-Surface Mapping

Wide-field corneoscleral mapping samples a larger and more asymmetric surface than central corneal mapping [4]. Landmark definition and levelling therefore become particularly consequential [5,6], while multi-gaze reconstruction adds dependence on gaze direction and overlap registration [7]. The Eye Surface Profiler uses Fourier-transform profilometry to measure the anterior eye beyond the central cornea, with accuracy and precision characterised on reference surfaces and human eyes [4]. Its wider field supports analysis of the limbus and sclera but requires explicit treatment of gaze, eyelid coverage, missing data and surface orientation [4–6].

Abass et al. developed a three-dimensional non-parametric limbus-detection method that identifies the corneoscleral transition from profile data without imposing a fixed parametric limbal shape [5]. A data-derived limbus can serve as a physical landmark for levelling and regional analysis because parametric eye models may misrepresent limbal position and shape [5,42].

In a study of scleral asymmetry, Abass et al. detected the limbus in three dimensions, levelled each eye surface to a best-fit limbal plane and applied processing to reduce peripheral edge artefact [6]. The method separates natural ocular orientation from the coordinate frame used to describe regional scleral height [6]. The chosen reference plane therefore affects how asymmetry is expressed and compared [6,42].

Consejo et al. examined the effect of corneal tilt on fitted asphericity and found that levelling the surface around an optical axis changed conic and biconic descriptors [24]. Asphericity values obtained from differently levelled surfaces or coordinate systems with different axial definitions should not be compared without qualification [24,38].

Eye tilt has also been associated with Scheimpflug densitometry, although the relationship is not a simple direct geometric effect [25]. In a healthy sample, age mediated the observed association between tilt and densitometry [25]. Densitometry differences should therefore not be attributed to tilt without considering age and the measurement model [25].

Multi-gaze stitching enlarges coverage by registering maps acquired in different gaze directions [7]. Lin et al. compared stitched Medmont Meridia maps with single-shot Eye Surface Profiler measurements in healthy participants and reported differences in central agreement and surface coverage [7]. Their findings support explicit validation of the stitching transformation, overlap region and peripheral reconstruction rather than assuming that a larger composite map is geometrically faithful [7].

A 2026 study of 131 astigmatic eyes found narrower limits of agreement for corneoscleral measurements at an 8 mm chord than at a 14 mm chord. Although the study examined

topographic consistency rather than induced misalignment, its findings show that uncertainty increases towards the periphery and that central-corneal tolerances should not be transferred uncritically to wide-field analyses [43].

Selected articles on ocular axes, levelling and wide-field mapping are summarised in Table 2.

Table 2. Selected articles on ocular axes, levelling and wide-field mapping.

Study	Surface or Landmark	Methodological Contribution	Relevance to Misalignment
Iskander et al., 2016 [4]	Cornea, limbus and visible sclera	Characterised the operating principle, accuracy and precision of the Eye Surface Profiler	Provides the measurement basis for wide-field levelling and gaze-dependent analysis
Abass et al., 2018: ocular axes [38]	Geometrical and visual axes	Mapped relative axis positions and described locating the visual centre from geometric references	Shows why centre and axis definitions must be explicit
Abass et al., 2018: limbus detection [5]	Three-dimensional limbal contour	Introduced a non-parametric limbus-detection method based on profile data	Enables landmark-based levelling without imposing a fixed parametric limbal shape
Abass et al., 2019 [6]	Corneoscleral point cloud and limbal plane	Levelled surfaces to a best-fit limbal plane and reduced peripheral edge artefact	Separates ocular orientation and processing artefact from expressed scleral asymmetry
Moore et al., 2020 [42]	Limbus represented by parametric eye models	Compared modelled and data-derived limbal geometry	Shows that an assumed landmark shape can bias levelling and regional analysis
Consejo et al., 2021 [24]	Anterior corneal surface	Quantified the effect of corneal tilt on fitted asphericity	Asphericity values depend on tilt treatment and axis definition
Consejo et al., 2022 [25]	Scheimpflug corneal densitometry	Analysed eye tilt and the mediating effect of age	Tilt-densitometry associations require age-aware interpretation
Lin et al., 2025 [7]	Multi-gaze stitched corneoscleral maps	Compared stitched profilometry with single-shot Eye Surface Profiler data	Stitching accuracy, overlap and peripheral coverage require validation

Note: Each row is based on the article cited in the first column.

6. Registration of Repeated Maps

Between-scan registration addresses a different problem from levelling a single acquisition [15,20]. It estimates the transformation that best aligns two measured surfaces before interpreting their differences as biological or treatment-related change [15,20]. Rigid-body methods commonly estimate three translations and three rotations, although the fitted region, distance metric and optimisation method vary [15,20,28].

Wang et al. developed iterative registration of overlapping videokeratography views [20]. Bao et al. subsequently estimated three translations and three rotations between paired Pentacam anterior and posterior surfaces from 124 healthy eyes [15]. In that study, the mean combined-surface RMS difference decreased from 8.46 ± 2.75 to 7.28 ± 2.58 µm (13.95%), while the anterior-surface difference fell from 4.58 ± 1.84 to 2.97 ± 1.29 µm (35.13%) [15]. Estimated x- and y-translation standard deviations were approximately 49 and 54 µm, while the angular component standard deviations were 0.41°, 0.37° and 2.35° [15]. The differences remaining after registration are important: a fitted transformation cannot remove segmentation uncertainty, tear-film effects or genuine focal change [15,28].

Tomography matching has also been applied after laser in situ keratomileusis (LASIK) and in keratoconus [21,22]. Estimated misalignment contributed to differences between

successive post-LASIK elevation maps [21]. In a separate Pentacam study, keratoconic eyes showed greater estimated misalignment and poorer repeatability than matched normal eyes [22]. A progression threshold should therefore be linked to disease state, platform, analysis diameter and registration method rather than borrowed from healthy eyes [22,41].

Schröder et al. proposed a framework that separates systematic differences, random precision and alignment components in corneal-shape measurements [28]. Their subsequent comparison of Pentacam HR, CASIA SS-1000 and TMS-5 data showed that the influence of alignment correction differed between measurement principles [8]. This device dependence argues against a universal correction factor or a single acceptable displacement threshold [8,40].

7. Device Dependence and Clinical Interpretation

Good within-device repeatability does not imply agreement between devices [44–46]. Orbscan II, Pentacam and Galilei can produce systematically different keratometric, power, elevation or pachymetric values despite acceptable repeatability within each instrument [44,45]. Swept-source OCT and rotating Scheimpflug tomography likewise show parameter-dependent agreement and repeatability in normal and keratoconic eyes [46]. Serial assessment should therefore use the same device, software version, scan mode and analysis settings whenever possible [40,44,46].

A 2025 comparison found high repeatability across the Eyestar 900, Pentacam AXL Wave, Anterion and MS-39, but agreement depended on the device pair, parameter and clinical group. Eyestar 900 was reported as interchangeable with Anterion and MS-39 in normal eyes and for selected parameters in keratoconic and post-refractive eyes, whereas agreement with Pentacam AXL Wave was limited. The study provides contextual evidence on platform agreement rather than direct evidence of misalignment and shows why repeatability alone cannot justify universal interchangeability [29]. A 2026 study of keratoconic eyes comparing Sirius Scheimpflug–Placido tomography with Anterion swept-source OCT likewise found parameter-dependent agreement and limits of agreement that were too wide to support interchangeable use [47].

Disease severity changes measurement uncertainty [22,41,45]. Pentacam repeatability deteriorates for several parameters as keratoconus advances, and inter-device agreement worsens in irregular corneas [41,45]. Alignment correction cannot compensate for weak signal, segmentation failure or an unstable fit on a highly irregular surface [28,41,46]. A 2025 MS-39 study of 208 keratoconic eyes similarly found that repeatability worsened with disease severity and that averaging three consecutive scans improved repeatability by about 44%, supporting severity-adapted, device-specific precision limits for progression assessment [48].

An asymmetric map does not necessarily indicate ectasia [12,23,49]. Astigmatic eyes can generate false-positive Scheimpflug ectasia classifications, and local epithelial irregularity can produce topographic patterns that simulate keratoconus [23,49]. When a map is unexpected, check geometric quality alongside refraction, slit-lamp findings, epithelial thickness, posterior elevation, and repeat imaging [12,23,49].

Tear-film dynamics are a separate but interacting source of error [16,17]. Videotopography can detect post-blink tear-film build-up and subsequent disruption, and keratometric reproducibility decreases as the interval after blinking increases [16,17]. Standardised blink timing and inspection of Placido mires should therefore accompany geometric quality control [16,17].

Accommodation and recent contact procedures should be considered separately rather than automatically attributed to misalignment. The accommodative protocol studied by

Bayramlar et al. did not produce a substantial mean change in topography, whereas gonioscopy produced small but detectable changes in some measurements [18,19].

Contact-lens wear is a more persistent pre-acquisition confounder. A 2025 systematic review found wide variation in the time required for corneal measurements to stabilise after lens cessation, with the interval depending on lens type, fit, wear pattern, age, and the imaging endpoint. A fixed waiting period is therefore difficult to defend; report lens history and evidence of stability for longitudinal or pre-operative imaging [50].

The clinical meaning of alignment depends on the chosen reference [10,26,38]. In an orthokeratology study, rotational misalignment was strongly associated with a shift in the measured treatment position. Still, treatment-centred corneal symmetry indices did not differ between visually and geometrically aligned scans [26]. This result is specific to the study context, but it illustrates why visual-axis, corneal-vertex and geometric-centre alignment should not be treated as interchangeable [26].

Progression criteria further complicate interpretation. A 2026 systematic review found that composite indices and global surface measures generally performed better than isolated single-point metrics for detecting keratoconus progression. Alignment control should therefore be treated as one component of a broader, multi-parameter assessment rather than a substitute [51]. A study published on 15 September 2026 found that peripheral pachymetric and eccentricity measures, together with composite tomographic-biomechanical indices, helped distinguish forme fruste or suspect keratoconus even when Kmax remained similar to normal eyes, further supporting a layered multi-parameter approach [52].

8. Artificial Intelligence in the Geometric Measurement Chain

The reviewed artificial intelligence literature principally addresses two clinical tasks: diagnostic discrimination using instrument-derived maps or indices, and longitudinal risk prediction based on repeated geometry-dependent measurements [30–37]. A third, distinct methodological task is the estimation and correction of acquisition-related geometric error. The available clinical evidence does not establish that the performance reported for the first two tasks transfers to the third. These applications should therefore be evaluated separately according to their measurement inputs and validation targets.

8.1. Diagnostic Discrimination from Geometry-Dependent Inputs

Studies using geometry-derived corneal inputs have achieved high discrimination under their selected sampling and testing designs. An artificial neural network trained on Placido-disc and anterior-segment OCT measurements from 6677 eyes, each from a different patient, reported 98.6% accuracy for keratoconus and 98.5% for keratoconus-suspect classification, although suspect recall was 69.7% [36]. A Galilei-map study involving 1411 eyes from 827 participants reported external-evaluation accuracies of 97.1–98.3% for selected convolutional networks [37]. These results should not be read as evidence of invariance to fixation, tilt, reference-surface selection or changes in instrument preprocessing [36,37].

The broader database scan added complementary evidence on how imaging modality and data representation condition model performance. A systematic review and meta-analysis that searched PubMed, Scopus and Web of Science reported modality-dependent diagnostic performance across Scheimpflug, Placido and combined imaging approaches [53]. This supports treating the acquisition platform and map construction as part of the model input rather than as a neutral preprocessing step. A 2026 Pentacam radiomics study of 415 eyes also showed clear modality dependence: posterior-elevation features performed best for early screening, whereas curvature- and elevation-derived features outperformed pachymetry for disease staging [54].

Engineering-oriented investigations further demonstrate the importance of representation. Lavric et al. reported up to 94% diagnostic accuracy from OCT-derived topographic, elevation and pachymetric descriptors [55]; a subsequent study reported areas under the receiver operating characteristic curve of 0.99 for keratoconus and 0.97 for early keratoconus using corresponding raw parameters [56]. KerNet analysed five raw Pentacam matrices, with attention mapping used to identify influential regions [57]. These reports evaluated classification from acquired geometry, but the reviewed results do not document a controlled physical challenge in which known fixation offsets, ocular pitch or yaw, or registration perturbations were applied to held-out clinical eyes.

Synthetic image augmentation should not be conflated with a controlled acquisition experiment. Qayyum et al. reported random horizontal reflection (probability 0.2) and rotations of up to 3° (probability 0.2) during training [37]. These transformations alter the rendered image rather than imposing measured changes in ocular pose with an independently known surface reference. The study included several scans and both eyes from individual participants, and explicitly stated that participant-level evaluation was not performed [37]. In addition, images from a separately sourced dataset were used for further training before subsequent validation and testing. The resulting performance figures are therefore informative but do not constitute an untouched, participant-independent external challenge of geometric robustness [37].

A more explicitly geometry-aware machine-learning study used the fellow eye as the reference surface for anterior elevation in 9230 raw Pentacam files and identified recurrent symmetry patterns described as flat, tilt, cone and four-leaf [58]. This approach shows that reference-surface choice can be incorporated into computational analysis, while also demonstrating that the resulting features are conditional on a defined coordinate relationship between the two eyes.

Reported performance remains conditional on sample definition and validation. In the single-centre analysis of Syta et al., 144 eye-level scans were used to compare models across tabular Pentacam feature groups; accuracies reached 96–98% in selected development analyses, whereas an independent held-out test described in the full report gave approximately 90% accuracy for the best models [32]. In a prospective five-centre study, the 1035 eyes represented 1035 individual participants, eliminating within-participant duplication across its sample-level partitions by design; the external-test AUROCs were 0.952 for forme fruste, 0.991 for subclinical disease and 1.000 for clinical disease [33]. Semi-supervised clustering of 25,816 OCT scans identified a morphometric transition group, of which 72.7% with longitudinal observations met consensus progression criteria [34]. Diagnostic discrimination, unsupervised clustering and future progression prediction measure different clinical properties and should not be summarised using headline accuracy alone.

8.2. Longitudinal Risk Prediction and the Unit of Validation

Progression prediction is particularly sensitive to the precision and dependence structure of repeated measurements. In a retrospective raw-Pentacam study, single-visit prediction yielded a mean AUROC of 0.59, increasing to 0.75 when serial measurements were used, although precision and F1 scores remained modest [31]. By contrast, a 2026 multimodal investigation included 7396 eyes from 3893 patients for model development and 963 eyes from 519 patients at a separate hospital for external evaluation [35]. Its internal training/test split was performed by patient, keeping longitudinal observations of the same person together; AUROC increased from 0.84 with baseline data to 0.93 when sequential visits were incorporated [35]. The reported triage pathway was simulated using retrospective data, not established by a prospective intervention trial. Validation of risk models must therefore

report participant-, eye- and scan-level counts, the split unit, calibration and the clinical consequences of missed progression [30,31,35,48].

8.3. Geometric Correction as a Validation Priority

The reviewed diagnostic and progression studies primarily evaluate measurements that have already been reconstructed or processed by an imaging device; they do not establish whether AI can recover a physically correct surface from a known acquisition displacement. Demonstrating geometric correction would require an independently characterised reference surface, imposed and measured translations and rotations, and assessment of residual error after correction. Testing should also include irregular and postoperative corneas, variation in fixation and ocular motion, and clinically relevant outcomes. An improvement in classification accuracy or agreement between fitted maps cannot, by itself, show that an acquisition artefact has been removed without altering genuine focal change [9,15,20].

8.4. Laterality, Augmentation and Validation Gaps

Corneal maps have directional meaning: nasal and temporal sectors, superior–inferior asymmetry, axis definitions and the signs of positional descriptors are tied to anatomical laterality [10,26,38]. A left-eye map cannot be regarded as equivalent to a right-eye map simply because a software image is mirrored. Studies should state whether laterality was retained, whether one eye was reflected into a common nasal–temporal frame, and whether axis-dependent labels and derived indices were transformed consistently. A random horizontal flip used for training [37] is a data-augmentation operation; it is neither documentation of a clinically defined right/left-eye harmonisation rule nor a test of robustness to gaze or tilt. Where these procedures are not specified, the resulting uncertainty should be recorded rather than inferred away.

Across AI applications, the unit of data partitioning is as consequential as the choice of model. Patient-level separation is explicit in the longitudinal model of Balal et al. [35] and follows from one eye per patient in the datasets of Alió Del Barrio et al. [36] and Du et al. [33]. For studies containing several eyes, visits or extracted map regions per patient, an eye-level or image-level random split cannot establish the absence of participant leakage unless grouping is explicitly described. The evidence matrix in Table 3 distinguishes confirmed practices from details not established by the reviewed reports. A stronger geometric validation design would hold out patients and devices, impose measured physical translations and rotations within relevant acquisition limits, assess laterality-defined transformations, and determine whether any correction preserves genuine focal disease signal [9,15].

Table 3. Selected AI studies by clinical task, partition design and geometric validation.

Study/Task	Data and Partition Unit	Geometry and Laterality	Testing/Key Result	Principal Limitation
Alió Del Barrio et al. [36]; diagnosis	6677 eyes/6677 patients; random 70/30 study division	No geometric image augmentation described; laterality handling not specified	Multicentre internal validation; 98.6% KC accuracy	Patient uniqueness limits correlated-eye leakage; physical pose robustness not tested
Qayyum et al. [37]; diagnosis	1411 eyes/827 participants; 5602 maps; map-level 60/20/20 division; participant-level evaluation not performed	Training: horizontal flip ($p = 0.2$) and rotation ($\leq 3°$, $p = 0.2$); anatomical laterality harmonisation not reported	A separately sourced Pentacam dataset was also used for training, followed by a further split; 97.1–98.3% accuracy reported	Unseen-patient external validation is not established; correlated maps and lack of physical pose testing limit inference

Table 3. *Cont.*

Study/Task	Data and Partition Unit	Geometry and Laterality	Testing/Key Result	Principal Limitation
Syta et al. [32]; diagnosis	144 eye-level scans; 80/20 split and fivefold CV; participant grouping not specified	Tabular variables; image rotation/ reflection not applicable to reported model	Single-centre; selected development accuracy 96–98%; held-out comparison ≈90%	Potential dependence and modest test sample limit certainty
Du et al. [33]; diagnosis	1035 eyes from 1035 participants; development plus external site testing	Input indices/clinical variables; map mirroring and physical pose challenge not described	Prospective five-centre external test; FFKC AUROC 0.952	One-eye-per-person design supports participant-level disjointness
Cohen-Tayar et al. [31]; progression	1218 labelled tests; serial model used 819 scans; group-wise split not established in available summary	Raw Pentacam parameters; physical pose testing not described	Cross-validation; AUROC 0.59 (single)/0.75 (serial)	Repeated visits demand explicit patient-disjoint evaluation
Balal et al. [35]; progression	7396 eyes/3893 patients internal; 963 eyes/ 519 patients external; patient-grouped folds	OCT, Placido and tabular input; laterality and posed misalignment stress tests not reported here	External-hospital evaluation; baseline AUROC 0.84; serial 0.93	Stronger splitting; simulated triage is not prospective impact evidence
Kandakji et al. [34]; clustering	25,816 scans/5005 patients; unsupervised clustering, not a conventional classifier split	Derived MS-39 indices; augmentation/lateral-ity rule not specified in this synthesis	Cross-system and longitudinal clinical comparisons	Does not establish pose-invariant disease clustering

Note: Synthetic geometric augmentation, right/left-eye harmonisation and physical misalignment testing are distinct procedures. AUROC, area under the receiver operating characteristic curve; CV, cross-validation; FFKC, forme fruste keratoconus; KC, keratoconus.

9. Practical Recommendations

Before acquisition, the operator should level the head and confirm stable fixation [9,12,13]. The lids should be positioned without pressure on the globe, and the interval from a complete blink should be standardised [16,17]. For wide-field profiling, gaze direction and the visibility of the limbus and sclera should be recorded because missing sectors and altered orientation affect levelling and stitching [5–7].

During acquisition, automated quality indicators should be supplemented by inspection of ring continuity, section-image completeness, detected landmarks and the displayed centre [2,3,5]. A scan that is clinically discordant or visibly off-axis should be repeated after repositioning rather than accepted solely because the software reports an acceptable quality score [8,9,12].

For longitudinal comparison, the same device and protocol should be used, and both unregistered and registered differences should be retained when registration forms part of the analysis [8,15,40]. The transformation model, fitted region, optimisation method and residual mismatch should be reported because each choice can affect the apparent change [15,20,28]. When treatment position or decentration is reported, the visual or geometric reference used for re-centring should also be stated [26].

For wide-field data, reports should state how the limbus was detected and which plane or axis was used for levelling [5,6]. For multi-gaze data, the report should describe how overlaps were registered and how peripheral edge artefacts were handled [7,42]. These details help distinguish anatomical asymmetry from coordinate-system and stitching effects [6,7].

Clinical interpretation should combine map quality with corroborating examination and should avoid diagnosing progression from a change smaller than the relevant within-device uncertainty [22,23,41,48]. A repeated, well-centred acquisition that reproduces the same abnormality provides stronger evidence than one isolated colour map [9,12]. An evidence-based clinical practice guideline published on 15 September 2026 similarly recommends combined clinical and tomographic criteria for progression assessment and individualised follow-up rather than reliance on a single parameter [59].

An AI report should identify the versioned algorithm, raw and derived inputs, device and scan mode, reference surface, centring and laterality conventions, preprocessing, rejection rules, and the population in which the operating threshold was evaluated. Splits should be explicitly defined at patient, eye and scan levels; where appropriate, calibration and external-device performance should be reported in addition to discrimination [30,33,35]. Model outputs should be reviewed alongside unregistered maps and clinical findings. A probability score without an applicable operating threshold and a defined clinical action does not establish clinical utility. Table 4 proposes minimum measurement-chain reporting information rather than a substitute for established AI reporting guidance.

Table 4. Proposed minimum acquisition and reporting information.

Domain	Minimum Information	Evidence Basis	Purpose
Instrument	Manufacturer, model, software version, scan mode, map type and analysis diameter	Values and alignment sensitivity differ by measurement principle [8,40].	Supports replication and discourages inappropriate device interchange
Centre and reference axis	Fixation target, acquisition axis, detected centre and any re-centring rule	Eccentric fixation and axis mismatch alter asymmetry and aberration estimates [10,12,38].	Defines the geometric meaning of reported decentration
Head, eye and gaze position	Head-levelling method, gaze direction and method used to detect tilt or rotation	Surface tilt, rotation and multi-gaze acquisition change expressed geometry [7,9,13].	Allows assessment of acquisition-related bias
Limbus and levelling	Limbus-detection method, fitted plane or axis, included sectors and handling of missing data	Landmark definition and levelling alter expressed corneoscleral shape [5,6,42].	Separates anatomical asymmetry from coordinate choice
Misalignment variable	Direction, magnitude, coordinate convention and method of induction or estimation	Translation and rotation have distinct, model-dependent effects [11,15,27].	Links an effect size to a defined transformation
Quality control	Mire or section-image inspection, automated score, rejection criteria, repeat rule and blink timing	Tear-film and capture-quality effects remain after geometric correction [16,17,28].	Prevents software acceptance from being treated as proof of validity
Registration and stitching	Transformation model, fitted region, overlap, optimiser, residual mismatch and edge processing	Registration reduces differences but can introduce model-dependent composites [7,15,20].	Makes computational correction reproducible and auditable
Longitudinal outcome	Exact parameter, device-specific repeatability, clinical threshold and corroborating examination	Repeatability varies with disease severity and parameter [22,23,41].	Reduces the risk of labelling statistical fluctuation as progression

Table 4. *Cont.*

Domain	Minimum Information	Evidence Basis	Purpose
Artificial intelligence model and validation	Model and software version; raw inputs; preprocessing and rejected scans; participant, eye and scan counts; split unit; calibration; operating threshold; device and site validation; geometric stress tests	Correlated observations, device signatures and acquisition shortcuts can inflate apparent performance [30,32,37]	Shows whether performance reflects transferable morphology and supports a defined clinical decision

Note: This author-proposed framework complements, but does not replace, established reporting standards [60–62]; it has not been validated as a consensus checklist.

Relationship to Established AI Reporting Standards

The proposed checklist extends, rather than replaces, established reporting guidance. The 2024 Checklist for Artificial Intelligence in Medical Imaging (CLAIM) covers image acquisition, preprocessing, partitioning and robustness [60]. TRIPOD + AI addresses the development and evaluation of clinical prediction models, including handling of correlated data, model evaluation and transparency [61]. STARD-AI addresses diagnostic test accuracy studies and their data, reference standards and testing design [62]. Table 5 identifies the narrower contribution of the present framework: geometric coordinate conventions, elevation reference surfaces, registration residuals, eye laterality and physically measured misalignment stress tests. Its principal advantage is a task-specific measurement audit; its limitation is that it has not undergone independent consensus development or prospective clinical validation.

Table 5. Relationship of the proposed geometric reporting framework to AI reporting guidelines.

Guidance	Primary Scope	Overlapping Reporting Requirements	Additional Geometric Focus/Limitation
CLAIM 2024 [60]	Medical imaging AI development and evaluation	Acquisition protocol, preprocessing, partition level, robustness, external testing	Does not prescribe corneal axes, limbal levelling, elevation reference parameters or pose perturbation units
TRIPOD + AI [61]	Clinical diagnostic/prognostic prediction models	Participants, missingness, predictors, handling of overfitting, testing and calibration	Adds corneal scan-to-patient grouping, visit-registration details and declared geometric target definitions
STARD-AI [62]	Diagnostic accuracy evaluations of AI index tests	Population selection, reference standard, index-test conduct and diagnostic performance	Adds a reproducible acquisition-frame and map-comparison audit
Present proposal (Table 4)	Geometry-dependent corneal imaging and AI	Compatible with all three but focused on measurement provenance	Explicit centres, transformations, fitted surfaces, residual errors, laterality and physical stress tests; not validated as consensus guidance

Note: This is a domain-specific comparison, not a formal scoring or appraisal of reporting guidelines. The present proposal should be used as a supplementary checklist and requires consensus and clinical validation.

10. Limitations and Research Priorities

The studies varied in device physics, imposed or estimated displacement, reference-surface choice, fitting zone, eye condition, analysis diameter and outcome definition [8,9,12,15,27]. Even numerical results from apparently similar experiments cannot necessarily be pooled without matched coordinates, landmark conventions and

error metrics. A universal limit for translation, rotation or tilt is consequently not supported by the present evidence; clinically relevant acceptance criteria should be developed for specified devices, tasks and populations.

Controlled fixation and ocular-rotation experiments were concentrated in 1994–2007 [9,12,13], while quantitative registration work matured in 2014–2019 [15,20,28]. More recent publications have examined multi-gaze surface construction, inter-device precision and AI-based diagnostic or progression modelling [7,29,35,43,50,51]. Most of these contributions are contextual to the correction of acquisition misalignment rather than controlled physical challenges in patients with abnormal corneal geometry. The synthesis follows a structured narrative approach rather than a fully systematic multi-database protocol, and selection and appraisal bias remain possible.

Several direct experiments used healthy eyes [9,12] or model surfaces [11], although the greatest clinical concern lies in irregular corneas and postoperative follow-up [22]. Disease-specific studies are therefore needed to separate true biological change from registration error across clinically used indices [22,41].

Some apparent conflicts in the literature reflect different questions rather than true disagreement. Rotation-dominated acquisition experiments and rigid surface-registration studies estimate different error components [9,15,20]. Likewise, limbal-plane levelling may be appropriate for anatomical surface description, whereas visual-axis or treatment-centred alignment may be more relevant to optical or therapeutic questions [6,26,38]. High within-device repeatability can also coexist with limited agreement between devices [29], and strong AI discrimination of manifest disease can coexist with weak single-scan prediction of progression [30–33]. The reference frame, correction method and performance claim should therefore match the intended clinical decision.

Future work should use measured, separately controlled translations, rotations, gaze changes and reference-surface perturbations on both healthy and irregular eyes [5–9,15]. Analyses should publish raw, unregistered data alongside fitted reference parameters, region masks, transforms and residuals, and report the effect of correction on clinically relevant thresholds, false positives and missed progression. AI studies should use patient-disjoint partitions, describe right/left-eye standardisation, distinguish synthetic augmentation from actual acquisition perturbation, and quantify robustness under withheld devices and held-out poses [33,35–37,60–62]. Prospective clinical impact, not lower surface RMS error or better retrospective AUROC alone, remains the decisive translational endpoint.

11. Conclusions

Geometric misalignment is best understood as a measurement-chain problem. Error can enter during acquisition, change with the selected centre or reference surface, persist after registration and pass into automated interpretation. No single correction fits every task: the relevant centre, axis, landmark, and transformation depend on whether the clinical question concerns optical quality, ectasia detection, treatment position, or longitudinal change.

In practice, acquisition quality remains the first safeguard. Clinical services should standardise fixation, head position, blink timing and scan acceptance, and should use the same platform for serial measurements whenever possible. When registration is used, reports should state the reference axis, transformation model, fitted region and residual mismatch. A change should be interpreted as progression or treatment response only when it is reproducible, exceeds the relevant measurement uncertainty and agrees with the clinical examination.

AI can inherit geometric uncertainty from the instruments and maps on which it is trained. Patient-disjoint testing, traceable reference surfaces, reproducible laterality

conventions and physically grounded perturbation tests are required before geometry-robust inference can be claimed. The next translational step is to establish whether these controls improve clinical decisions without concealing true localised change.

Supplementary Materials: The following supporting information can be downloaded at: https://www.mdpi.com/article/10.3390/ijtm6040055/s1, Supplementary Table S1. Database-specific search strategies used in the literature review.

Author Contributions: Conceptualisation, R.A. and A.A.; methodology, R.A. and A.A.; software, J.D. and A.A.; validation, J.T., A.J. and A.A.; formal analysis, R.A. and A.A.; investigation, R.A., J.T., J.D., A.J. and A.A.; resources, A.J. and A.A.; data curation, R.A. and A.A.; writing—original draft preparation, R.A., J.T., J.D., A.J. and A.A.; writing—review and editing, A.J. and A.A.; visualisation, J.D. and A.A.; supervision, A.J. and A.A.; project administration, A.J. and A.A. All authors have read and agreed to the published version of the manuscript.

Funding: This research received no external funding.

Institutional Review Board Statement: Not applicable.

Informed Consent Statement: Not applicable.

Data Availability Statement: No new data were created or analysed in this study. Data sharing does not apply to this review article.

Conflicts of Interest: The authors declare no conflicts of interest.

References

1. Fan, R.; Chan, T.; Prakash, G.; Jhanji, V. Applications of corneal topography and tomography: A review. *Clin. Exp. Ophthalmol.* **2018**, *46*, 133–146. [CrossRef]
2. Martin, R. Cornea and anterior eye assessment with Placido-disc keratoscopy, slit scanning evaluation topography and Scheimpflug imaging tomography. *Indian J. Ophthalmol.* **2018**, *66*, 360–366. [CrossRef]
3. Kanclerz, P.; Khoramnia, R.; Wang, X. Current developments in corneal topography and tomography. *Diagnostics* **2021**, *11*, 1466. [CrossRef]
4. Iskander, D.; Wachel, P.; Simpson, P.; Consejo, A.; Jesus, D. Principles of operation, accuracy and precision of an Eye Surface Profiler. *Ophthalmic Physiol. Opt.* **2016**, *36*, 266–278. [CrossRef]
5. Abass, A.; Lopes, B.; Eliasy, A.; Wu, R.; Jones, S.; Clamp, J.; Ambrósio, R.J.; Elsheikh, A. Three-dimensional non-parametric method for limbus detection. *PLoS ONE* **2018**, *13*, e0207710. [CrossRef]
6. Abass, A.; Lopes, B.; Eliasy, A.; Salomao, M.; Wu, R.; White, L.; Jones, S.; Clamp, J.; Ambrósio, R.J.; Elsheikh, A. Artefact-free topography based scleral-asymmetry. *PLoS ONE* **2019**, *14*, e0219789. [CrossRef]
7. Lin, W.-P.; Wu, L.-Y.; Lin, W.-R.; White, L.; Wu, R.; Fathy, A.; Alanazi, R.; Davies, J.; Abass, A. To Stitch or Not to Stitch, That Is the Question: Multi-Gaze Eye Topography Stitching Versus Single-Shot Profilometry. *Photonics* **2025**, *12*, 318. [CrossRef]
8. Schröder, S.; Maurer, S.; Eppig, T.; Seitz, B.; Rubly, K.; Langenbucher, A. Comparison of corneal tomography: Repeatability, precision, misalignment, mean elevation, and mean pachymetry. *Curr. Eye Res.* **2018**, *43*, 709–716. [CrossRef]
9. Hick, S.; Laliberte, J.; Meunier, J.; Chagnon, M.; Brunette, I. Effects of misalignment during corneal topography. *J. Cataract. Refract. Surg.* **2007**, *33*, 1522–1529. [CrossRef]
10. Salmon, T.; Thibos, L. Videokeratoscope-line-of-sight misalignment and its effect on measurements of corneal and internal ocular aberrations. *J. Opt. Soc. Am. A Opt. Image Sci. Vis.* **2002**, *19*, 657–669. [CrossRef]
11. Wang, J.; Rice, D.; Klyce, S. Analysis of the effects of astigmatism and misalignment on corneal surface reconstruction from photokeratoscopic data. *Refract. Corneal Surg.* **1991**, *7*, 129–140. [CrossRef]
12. Hubbe, R.; Foulks, G. The effect of poor fixation on computer-assisted topographic corneal analysis: Pseudokeratoconus. *Ophthalmology* **1994**, *101*, 1745–1748. [CrossRef]
13. Douthwaite, W.; Pardhan, S. Surface tilt measured with the EyeSys videokeratoscope: Influence on corneal asymmetry. *Investig. Ophthalmol. Vis. Sci.* **1998**, *39*, 1727–1735.
14. Buehren, T.; Lee, B.; Collins, M.; Iskander, D. Ocular microfluctuations and videokeratoscopy. *Cornea* **2002**, *21*, 346–351. [CrossRef]
15. Bao, F.; Wang, J.; Huang, J.; Yu, Y.; Deng, M.; Li, L.; Yu, A.; Wang, Q.; Davey, P.; Elsheikh, A. Effect of misalignment between successive corneal videokeratography maps on the repeatability of topography data. *PLoS ONE* **2015**, *10*, e0139541. [CrossRef]

16. Nemeth, J.; Erdelyi, B.; Csakany, B.; Gaspar, P.; Soumelidis, A.; Kahlesz, F.; Lang, Z. High-speed videotopographic measurement of tear film build-up time. *Investig. Ophthalmol. Vis. Sci.* **2002**, *43*, 1783–1790.
17. Erdelyi, B.; Csakany, B.; Nemeth, J. Reproducibility of keratometric measurements decreases with time after blinking. *Eur. J. Ophthalmol.* **2006**, *16*, 371–375. [CrossRef]
18. Bayramlar, H.; Sadigov, F.; Yildirim, A. Effect of accommodation on corneal topography. *Cornea* **2013**, *32*, 1251–1254. [CrossRef]
19. George, M.; Kuriakose, T.; DeBroff, B.; Emerson, J. The effect of gonioscopy on keratometry and corneal surface topography. *BMC Ophthalmol.* **2006**, *6*, 26. [CrossRef]
20. Wang, J.; Elsheikh, A.; Davey, P.; Wang, W.; Bao, F.; Mottershead, J. Corneal topography matching by iterative registration. *Proc. Inst. Mech. Eng. Part H J. Eng. Med.* **2014**, *228*, 1154–1167. [CrossRef]
21. Zheng, X.; Yang, W.; Huang, L.; Wang, J.; Cao, S.; Geraghty, B.; Zhao, Y.; Wang, Q.; Bao, F.; Elsheikh, A. Evaluating the repeatability of corneal elevation through calculating the misalignment between successive topography measurements during the follow up of LASIK. *Sci. Rep.* **2017**, *7*, 3122. [CrossRef]
22. Zheng, Y.; Huang, L.; Zhao, Y.; Wang, J.; Zheng, X.; Huang, W.; Geraghty, B.; Wang, Q.; Chen, S.; Bao, F.; et al. Repeatability of corneal elevation maps in keratoconus patients using the tomography matching method. *Sci. Rep.* **2017**, *7*, 17457. [CrossRef]
23. Henriquez, M.; Hadid, M.; Moctezuma, C.; Izquierdo, L.; Binder, P. The false positive rates for detecting keratoconus and potential ectatic corneal conditions when evaluating astigmatic eyes with Scheimpflug technology. *Eur. J. Ophthalmol.* **2022**, *32*, 2532–2546. [CrossRef]
24. Consejo, A.; Fathy, A.; Lopes, B.; Ambrósio, R.J.; Abass, A. Effect of Corneal Tilt on the Determination of Asphericity. *Sensors* **2021**, *21*, 7636. [CrossRef]
25. Consejo, A.; Jiménez-García, M.; Rozema, J.; Abass, A. Influence of eye tilt on corneal densitometry. *Ophthalmic Physiol. Opt.* **2022**, *42*, 1032–1037. [CrossRef]
26. Eltantawy, E.; Field, E.; Bui, C.; Kang, M. Orthokeratology Decentration: Topography Alignment, Tear Profile Symmetry and Induced HOAs. *Ophthalmic Physiol. Opt.* **2026**, *46*, 366–378. [CrossRef]
27. Deng, M.; Li, L.; Huang, L.; Wang, W.; Yu, A.; Huang, J.; Wang, Q.; Bao, F.; Elsheikh, A. Effect of translation and rotation fitting on analysis of corneal topography. *J. Med. Eng. Technol.* **2015**, *39*, 309–315. [CrossRef]
28. Schröder, S.; Eppig, T.; Langenbucher, A. A concept for the analysis of repeatability and precision of corneal shape measurements. *Z. Med. Phys.* **2016**, *26*, 150–158. [CrossRef]
29. Kundu, G.; Shetty, N.; Modak, D.; Kaweri, L.; Khamar, P.; Arora, V.; Nuijts, R.M.M.A.; Shetty, R. Repeatability and agreement of a new anterior segment optical coherence tomography with standard devices in normal, keratoconus, and post-refractive eyes. *Indian J. Ophthalmol.* **2025**, *73*, 325–334. [CrossRef]
30. Tiong, E.W.W.; Liu, S.-H.; Ting, D.S.J. Cochrane corner: Artificial intelligence for keratoconus. *Eye* **2024**, *38*, 3406–3408. [CrossRef]
31. Cohen-Tayar, Y.; Cohen, H.; Key, D.; Tiosano, A.; Rozanes, E.; Livny, E.; Bahar, I.; Nahum, Y. Machine learning-based identification of risk factors of keratoconus progression using raw corneal tomography data. *Cornea* **2025**, *44*, 605–612. [CrossRef]
32. Syta, A.; Podkowiński, A.; Chorągiewicz, T.; Karpiński, R.; Gęca, J.; Wróbel-Dudzińska, D.; Jonak, K.E.; Głuchowski, D.; Maciejewski, M.; Rejdak, R.; et al. Machine learning-assisted early detection of keratoconus: A comparative analysis of corneal topography and biomechanical data. *Sci. Rep.* **2025**, *15*, 24399. [CrossRef]
33. Du, K.; Peng, R.; Chen, Y.; Yuan, B.; Wu, H.; Chen, T.; Zhu, J.; Zu, X.; Wang, J.; Cui, J.; et al. Enhancing early keratoconus detection with multimodal machine learning: Integrating tomography, biomechanics, and clinical risk factors. *Am. J. Ophthalmol.* **2025**, *280*, 334–346. [CrossRef]
34. Kandakji, L.; Balal, S.; Stupnicki, A.; Liu, S.; Leucci, M.; Gore, D.; Allan, B.; Pontikos, N. Data-driven detection of subclinical keratoconus via semi-supervised clustering of multidimensional corneal biomarkers. *Ophthalmol. Sci.* **2026**, *6*, 100998. [CrossRef]
35. Balal, S.; Kandakji, L.; Leucci, M.; Keane, P.A.; Gore, D.; Pontikos, N.; Allan, B.D. Automated triage for new keratoconus referrals using multimodal deep learning. *Ophthalmol. Sci.* **2026**, *6*, 101208. [CrossRef]
36. Alió Del Barrio, J.L.; Eldanasoury, A.M.; Arbelaez, J.; Faini, S.; Versaci, F. Artificial neural network for automated keratoconus detection using a combined Placido disc and anterior segment optical coherence tomography topographer. *Transl. Vis. Sci. Technol.* **2024**, *13*, 13. [CrossRef]
37. Qayyum, S.; Arshad, M.; Saeed, H. Artificial intelligence for diagnosis of keratoconus using Scheimpflug based corneal tomography. *Int. J. Ophthalmol.* **2026**, *19*, 1221–1234. [CrossRef]
38. Abass, A.; Vinciguerra, R.; Lopes, B.; Bao, F.; Vinciguerra, P.; Ambrósio, R.J.; Elsheikh, A. Positions of Ocular Geometrical and Visual Axes in Brazilian, Chinese and Italian Populations. *Curr. Eye Res.* **2018**, *43*, 1404–1414. [CrossRef]
39. Campos-Garcia, M.; Aguirre-Aguirre, D.; Moreno-Oliva, V.; Huerta-Carranza, O.; Armengol-Cruz, V. Measurement and correction of misalignments in corneal topography using the null-screen method. *OSA Contin.* **2021**, *4*, 158–170. [CrossRef]

40. Schröder, S.; Langenbucher, A.; Schrecker, J. Comparison of corneal elevation and pachymetry measurements made by two state-of-the-art corneal tomographers with different measurement principles. *PLoS ONE* **2019**, *14*, e0223770. [CrossRef]
41. Kreps, E.O.; Jiménez-García, M.; Issarti, I.; Claerhout, I.; Koppen, C.; Rozema, J.J. Repeatability of the Pentacam HR in various grades of keratoconus. *Am. J. Ophthalmol.* **2020**, *219*, 154–162. [CrossRef]
42. Moore, J.; Shu, X.; Lopes, B.; Wu, R.; Abass, A. Limbus misrepresentation in parametric eye models. *PLoS ONE* **2020**, *15*, e0236096. [CrossRef]
43. Xiang, Z.; Han, D.; Gu, D.; Qian, Y.; Chen, Z. Comparison of corneoscleral topographic consistency in eyes with low-to-moderate and high astigmatism. *Contact Lens Anterior Eye* **2026**, *49*, 102688. [CrossRef]
44. Crawford, A.Z.; Patel, D.V.; McGhee, C.N.J. Comparison and repeatability of keratometric and corneal power measurements obtained by Orbscan II, Pentacam, and Galilei corneal tomography systems. *Am. J. Ophthalmol.* **2013**, *156*, 53–60. [CrossRef]
45. Meyer, J.J.; Gokul, A.; Vellara, H.R.; Prime, Z.; McGhee, C.N.J. Repeatability and agreement of Orbscan II, Pentacam HR, and Galilei tomography systems in corneas with keratoconus. *Am. J. Ophthalmol.* **2017**, *175*, 122–128. [CrossRef]
46. Herber, R.; Lenk, J.; Pillunat, L.E.; Raiskup, F. Comparison of corneal tomography using a novel swept-source optical coherence tomographer and rotating Scheimpflug system in normal and keratoconus eyes: Repeatability and agreement analysis. *Eye Vis.* **2022**, *9*, 19. [CrossRef]
47. Erdogan, K.; Unlu, M.; Ozer, F. Agreement between Sirius Scheimpflug-Placido tomography and Anterion swept-source OCT in keratoconic eyes stratified by prior corneal cross-linking: A retrospective cross-sectional agreement study. *Int. Ophthalmol.* **2026**, *46*, 393. [CrossRef]
48. Balal, S.; Cai, Y.; Kandakji, L.; Liu, S.; Mullholand, P.J.; Leucci, M.; Pontikos, N.; Gore, D.; Allan, B. Establishing the ground truth for keratoconus progression: Combining repeated measures and adapting precision limits to disease severity in corneal tomography. *J. Cataract. Refract. Surg.* **2025**, *51*, 790–798. [CrossRef]
49. El Wardani, M.; Hashemi, K.; Aliferis, K.; Kymionis, G. Topographic changes simulating keratoconus in patients with irregular inferior epithelial thickening documented by anterior segment optical coherence tomography. *Clin. Ophthalmol.* **2019**, *13*, 2103–2110. [CrossRef]
50. Abid, A.; Kandel, H.; Watson, S. Systematic review investigating the time taken for corneal stabilisation following contact lens cessation. *Br. J. Ophthalmol.* **2025**, *109*, 1099–1108. [CrossRef]
51. Gil, P.; d'Almeida, O.C.; Cunha, B.; Gil, J.Q.; Donato, H.; Alves, N.; Rosa, A.; Murta, J. Criteria for keratoconus progression: A systematic review of diagnostic test accuracy. *Cornea* **2026**, *45*, 387–395. [CrossRef]
52. Zhang, W.; Li, A.; Jiang, H.; Wei, Y.; Feng, J.; Li, S.; Jiang, Y.; Jie, Y. Peripheral pachymetry, eccentricity, and composite tomographic-biomechanical indices for screening forme fruste/suspect keratoconus. *BMC Ophthalmol.* **2026**. [CrossRef]
53. Hashemi, H.; Doroodgar, F.; Niazi, S.; Khabazkhoob, M.; Heidari, Z. Comparison of different corneal imaging modalities using artificial intelligence for diagnosis of keratoconus: A systematic review and meta-analysis. *Graefe's Arch. Clin. Exp. Ophthalmol.* **2024**, *262*, 1017–1039. [CrossRef]
54. Gong, Q.; Dai, Y.; Wang, W.; Wang, D.; Fang, L.; Li, J. Pentacam multimodal topography-based radiomics for early keratoconus screening and staging. *Sci. Rep.* **2026**, *16*, 61768. [CrossRef]
55. Lavric, A.; Popa, V.; Takahashi, H.; Yousefi, S. Detecting Keratoconus From Corneal Imaging Data Using Machine Learning. *IEEE Access* **2020**, *8*, 149113–149121. [CrossRef]
56. Lavric, A.; Anchidin, L.; Popa, V.; Al-Timemy, A.H.; Alyasseri, Z.A.A.; Takahashi, H.; Yousefi, S.; Hazarbassanov, R.M. Keratoconus Severity Detection From Elevation, Topography and Pachymetry Raw Data Using a Machine Learning Approach. *IEEE Access* **2021**, *9*, 84344–84355. [CrossRef]
57. Feng, R.; Xu, Z.; Zheng, X.; Hu, H.; Jin, X.; Chen, D.Z.; Yao, K.; Wu, J. KerNet: A Novel Deep Learning Approach for Keratoconus and Sub-Clinical Keratoconus Detection Based on Raw Data of the Pentacam HR System. *IEEE J. Biomed. Health Inform.* **2021**, *25*, 3898–3910. [CrossRef]
58. Mehravaran, S.; Dehzangi, I.; Rahman, M.M. Interocular Symmetry Analysis of Corneal Elevation Using the Fellow Eye as the Reference Surface and Machine Learning. *Healthcare* **2021**, *9*, 1738. [CrossRef]
59. Bustamante-Arias, A.; Rosas-Apraez, A.; Restrepo, C.A.; Lizarazo, M.I.; Tawse-Smith, D.; Carreño, N.I.; Holguin, L.D.; Gatinel, D.; Romero, M.; Rocha, L.G.; et al. Evidence-Based Clinical Practice Guideline for Diagnosis, Treatment, and Follow-Up of Keratoconus Patients. *Clin. Ophthalmol.* **2026**, *20*, 612713. [CrossRef]
60. Tejani, A.S.; Klontzas, M.E.; Gatti, A.A.; Mongan, J.T.; Moy, L.; Park, S.H.; Kahn, C.E., Jr.; CLAIM 2024 Update Panel. Checklist for Artificial Intelligence in Medical Imaging (CLAIM): 2024 Update. *Radiol. Artif. Intell.* **2024**, *6*, e240300. [CrossRef]

61. Collins, G.S.; Moons, K.G.M.; Dhiman, P.; Riley, R.D.; Beam, A.L.; Van Calster, B.; Ghassemi, M.; Liu, X.; Reitsma, J.B.; van Smeden, M.; et al. TRIPOD+AI statement: Updated guidance for reporting clinical prediction models that use regression or machine learning methods. *BMJ* **2024**, *385*, e078378, Erratum in *BMJ* **2024**, *385*, q902. https://doi.org/10.1136/bmj-2023-078378. [CrossRef]
62. Sounderajah, V.; Guni, A.; Liu, X.; Collins, G.S.; Karthikesalingam, A.; Markar, S.R.; Golub, R.M.; Denniston, A.K.; Shetty, S.; Moher, D.; et al. The STARD-AI reporting guideline for diagnostic accuracy studies using artificial intelligence. *Nat. Med.* **2025**, *31*, 3283–3289, Correction in *Nat. Med.* **2026**, *32*, 3493. https://doi.org/10.1038/s41591-025-03953-8. [CrossRef]

Disclaimer/Publisher's Note: The statements, opinions and data contained in all publications are solely those of the individual author(s) and contributor(s) and not of MDPI and/or the editor(s). MDPI and/or the editor(s) disclaim responsibility for any injury to people or property resulting from any ideas, methods, instructions or products referred to in the content.